AD-A110 657 MASSACHUSETTS INST OF TECH CAMBRIDGE F/G 11/6
THE AGING AND TEMPERING OF IRON-NICKEL-CARBON-MARTENSITES.(U)
DEC 81 A SHERMAN, G T ELDIS, M COHEN N00014-81-K-0613
UNCLASSIFIED TR-5 NL

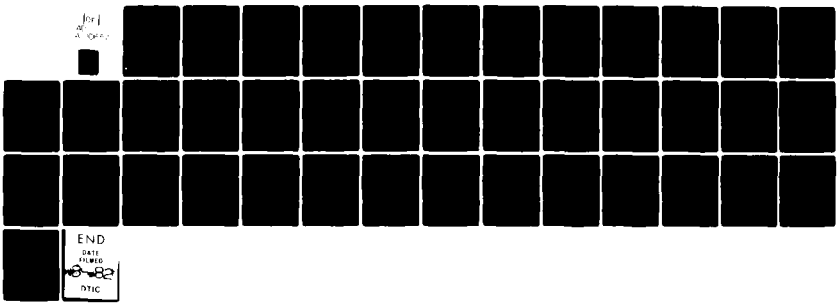

END
DATE FILMED
3-82
DTIC

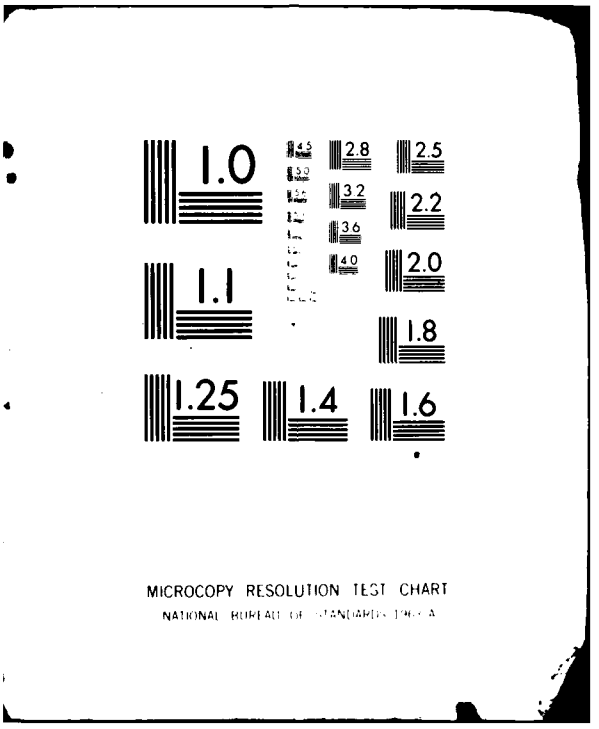
1.0
1.1
1.25
1.4
1.6
1.8
2.0
2.2
2.5
2.8
3.2
3.6
4.0
4.5
5.0
MICROCOPY RESOLUTION TEST CHART
NATIONAL BUREAU OF STANDARDS 1963-A

LEVEL II

AD A110657

DTIC FILE COPY

SECURITY CLASSIFICATION OF THIS PAGE (When Data Entered)

REPORT DOCUMENTATION PAGE	READ INSTRUCTIONS BEFORE COMPLETING FORM
1. REPORT NUMBER: Technical Report No. 5, 1980-81	2. GOVT ACCESSION NO.: AD-A110 657
	3. RECIPIENT'S CATALOG NUMBER:
4. TITLE (and Subtitle): "The Aging and Tempering of Iron-Nickel-Carbon-Martensites"	5. TYPE OF REPORT & PERIOD COVERED: Technical Report; Oct. 1980 Sept. 1981
	6. PERFORMING ORG. REPORT NUMBER:
7. AUTHOR(s): A. Sherman, G. T. Eldis, and Morris Cohen	8. CONTRACT OR GRANT NUMBER(s): N00014-81-K-0013
9. PERFORMING ORGANIZATION NAME AND ADDRESS: Massachusetts Institute of Technology Cambridge, MA 02139	10. PROGRAM ELEMENT, PROJECT, TASK AREA & WORK UNIT NUMBERS:
11. CONTROLLING OFFICE NAME AND ADDRESS: Office of Naval Research Arlington, VA 22217	12. REPORT DATE: 31 December 1981
	13. NUMBER OF PAGES: 38
14. MONITORING AGENCY NAME & ADDRESS(if different from Controlling Office)	15. SECURITY CLASS. (of this report): Unclassified
	15a. DECLASSIFICATION/DOWNGRADING SCHEDULE:

16. DISTRIBUTION STATEMENT (of this Report)

Unlimited

DTIC ELECTE FEB 0 8 1982 E

17. DISTRIBUTION STATEMENT (of the abstract entered in Block 20, if different from Report)

18. SUPPLEMENTARY NOTES

To be published in Metallurgical Transactions as part of the Peter G. Winchell Memorial Symposium on Tempering, held in Louisville, Kentucky, October 1981.

19. KEY WORDS (Continue on reverse side if necessary and identify by block number)

Virgin martensites, aging, tempering, structural changes, kinetics

20. ABSTRACT (Continue on reverse side if necessary and identify by block number)

The aging and tempering of freshly quenched (M_s > RT) and virgin (M_s < RT) martensites with lath and plate morphologies in Fe-Ni-C alloys have been studied to obtain kinetic and structural information. At subambient temperatures, the first change is attributed to isothermal conversion of a small amount of retained austenite or to slight relaxations in the martensite, but this is not a significant part of the martensite aging process. Aging above -40°C to about 70°C is accompanied by the diffusion-controlled clustering

DD FORM 1 JAN 73 1473 EDITION OF 1 NOV 65 IS OBSOLETE
S/N 0102-014-6601

SECURITY CLASSIFICATION OF THIS PAGE (When Data Entered)

of carbon atoms, resulting in an increase in electrical resistivity proportional to the carbon content but independent of the martensitic morphology. This regime is followed above 100°C by the precipitation of ε-carbide (i.e., the conventional first stage of tempering), which may emerge directly from the carbon-rich clusters. At still higher temperatures, cementite forms separately (i.e., the conventional third stage of tempering) in competition with the ε-carbide. These two precipitation processes overlap, and their kinetics appear to be controlled by iron-atom diffusion away from the growing carbide particles along dislocation paths. No evidence was found in this investigation for a regime reflecting carbon migration to dislocations or other defects, but this possibility is not ruled out by the experimental methods employed.

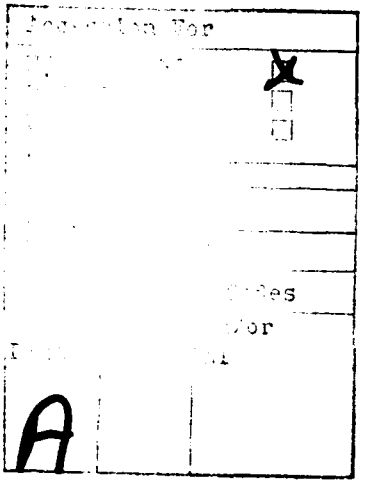

THE AGING AND TEMPERING OF IRON-NICKEL-CARBON-MARTENSITES*

by

A. M. Sherman, G. T. Eldis, and Morris Cohen

Abstract

The aging and tempering of freshly quenched (M_s > RT) and virgin (M_s < RT) martensites with lath and plate morphologies in Fe-Ni-C alloys have been studied to obtain kinetic and structural information. At subambient temperatures, the first change is attributed to isothermal conversion of a small amount of retained austenite or to slight relaxations in the martensite, but this is not a significant part of the martensite aging process. Aging above -40°C to about 70°C is accompanied by the diffusion-controlled clustering of carbon atoms, resulting in an increase in electrical resistivity proportional to the carbon content but independent of the martensitic morphology. This regime is followed above 100°C by the precipitation of ε-carbide (i.e., the conventional first stage of tempering), which may emerge directly from the carbon-rich clusters. At still higher temperatures, cementite forms separately (i.e., the conventional third stage of tempering) in competition with the ε-carbide. These two precipitation processes overlap, and their kinetics appear to be controlled by iron-atom diffusion away from the growing carbide particles along dislocation paths. No evidence was found in this investigation for a regime reflecting carbon migration to dislocations or other defects, but this possibility is not ruled out by the experimental methods employed.

---

* Prepared for the Peter G. Winchell Symposium on Tempering of Steel, TMS-AIME Fall Meeting, 12-13 October, 1981, Louisville, KY.

A. M. Sherman is Principal Research Scientist Associate, Ford Motor Company, Dearborn, MI 48121. G. T. Eldis is Research Manager, Climax Molybdenum Company of Michigan, Ann Arbor, MI 48106. Morris Cohen is Institute Professor Emeritus, Massachusetts Institute of Technology, Cambridge, MA 02139.

1. Introduction

Because of the wide range of mechanical properties obtainable through the hardening and tempering of steel, the structures of iron-carbon martensites and their decomposition products have been of lasting interest to metallurgists. Crystallographic and kinetic theories have been developed to account for the formation of ferrous martensite in its various forms, and numerous studies have identified several stages of decomposition during the tempering of martensite. Since there are excellent review papers available dealing with these topics, only a brief description of certain pertinent aspects will be given here[1-4].

Two major morphological types of ferrous martensite have been observed. As shown in Fig. 1, alloys with high M_s temperatures tend to form martensites consisting of packets of lath-shaped units containing highly dislocated regions. Alloys with lower M_s temperatures tend to form plate-like morphologies containing fine internal twins. The latter martensites are usually associated with significant amounts of retained austenite, while the lath martensites typically retain relatively little austenite. Some alloys transform to martensites with hybrid or mixed morphologies, such as irregular plates which are only partially twinned. These intermediate cases suggest that the transition from the lath morphology (where the lattice-invariant shear involved in the transformation occurs by slip) to the plate morphology (where twinning is the lattice-invariant shear mode) is not abrupt. It has been proposed that a change in the relative ease of slip vs. twinning is responsible for this transition in martensite morphology[5,6].

Since ferrous martensites form at such a fast rate and because the solubility of interstitial elements, such as carbon, is much greater in austenite than in body-centered iron, the transformation traps interstitials in metastable positions in the martensite. The changes which occur during the aging or tempering of martensite consist largely of the movements of carbon atoms from their as-quenched sites to lower-energy locations. Martensite which has not been subjected to any intentional aging treatment is often termed "freshly quenched." However, there is now substantial evidence that even at subambient temperatures, and also during the quenching of alloys with high M_s

temperatures, carbon movements and/or other changes take place. Speich[7] has calculated that carbon atoms in high M_s martensites can diffuse out of their initial sites to lattice defects before room temperature is reached. Data obtained from Mössbauer measurements[8-11], x-ray diffraction studies[12,13], electron microscopy[14-16], and field ion microscopy[17] provide experimental evidence of carbon redistribution in as-quenched martensites at temperatures as low as -40°C. Although the details may differ, the general interpretation of these results is that a carbon-clustering reaction preceding the first stage of tempering is the principal cause of the observed aging effects. These observations, however, have offered comparatively little information concerning the kinetics of such martensite aging. Thus, because most earlier investigations of tempering have used alloys with high M_s temperatures and/or have involved storage of the martensitic specimens at room temperature before measurements, it appears that no studies of the entire tempering sequence have started with the virgin (unaged) martensitic state. Likewise, the influence of martensite morphology on tempering behavior has not been specifically examined. In this regard, the role of dislocation substructure during low-temperature aging is of particular interest in light of two, possibly competing, phenomena which may occur, namely carbon-cluster formation and carbon trapping by lattice defects.

In the present investigation, electrical resistivity measurements were adopted to determine the overall aging and tempering kinetics of Fe-Ni-C martensites. In addition, optical and electron microscopy and x-ray diffraction were employed to correlate the kinetic data with the underlying structural changes. The alloy compositions and experimental techniques were chosen to insure that the above observations started with virgin martensites and that no inadvertent aging took place during the aging runs. Alloys with both lath and plate types of martensite, as well as some forming mixed morphologies, were included in this study in order to discern the effect of these structural differences on the aging and tempering behavior. (For the sake of easy discussion, we shall refer to the time/temperature phenomena as "aging" if they occur prior to the conventional first stage of tempering.)

2. Experimental Procedures

Three series of Fe-Ni-C alloys were designed for this study and prepared by the United States Steel Corporation. The series had 18, 21 and 24 weight percent nickel, with a range of carbon contents such that the martensitic morphologies generated in each series ranged from lath to mixed to plate. The nickel contents were selected because such alloys have low M_s temperatures, thus helping to minimize autotempering. Table I lists the compositions, estimated M_s temperatures, and martensite morphologies of the alloys.

The alloys were received as hot-rolled bars and were then cold worked and machined into rods and wires of appropriate sizes for the experiments. All these materials were given 24-hour homogenizing treatments at 1200°C in a protective atmosphere.

The resistivity specimens were prepared by spot welding two leads of pure nickel wire to each end of wire specimens 0.79 or 1.52 mm in diameter. These samples were austenitized in an argon atmosphere and quenched from a specially designed furnace by using pressurized gas to fire the specimen out of the austenitizing zone into an iced-brine quenching bath. Each such sample was immediately transferred from the brine to liquid nitrogen to complete the quench and for storage until use.

Aging or tempering of the martensitic specimens was accomplished by up-quenching from the liquid-nitrogen storage bath to a bath maintained at the desired temperature to within $\pm$ 2°C. At intervals, the specimens were transferred back to liquid-nitrogen baths for electrical resistance measurements, made with a Kelvin double bridge to a sensitivity of $\pm$ 0.1% of the absolute resistance of the specimens, or about 10^{-5} ohms. The resistance values were converted to electrical resistivities, which were then corrected for the presence of retained austenite, as described in Appendix A. The data are thus plotted as resistivity of 100% martensite at -196°C vs aging or tempering time at various temperatures.

For electron microscopy, disc samples were cut from 5 mm diameter rods, which had been quenched and tempered in the same ways as the resistivity specimens. Foils were prepared by electropolishing in a bath consisting of 1g anhydrous sodium chromate in 5 ml. glacial acetic acid. Inasmuch as the foil preparation had to be performed at or near room temperature, microscopic observations of virgin martensite could not be obtained.

An oscillating crystal technique[18,19] was employed to determine the tetragonality of the virgin and aged martensites. This method relied on the preparation and orientation of an austenite single crystal at room temperature; consequently such measurements were made only on alloys having subambient M_s temperatures. The austenitic specimens were subcooled in the x-ray apparatus to form virgin martensite. In-situ measurements of the tetragonality were carried out, and this was then followed by aging at temperatures from 20 to 350°C.

3. Results

Examples of complete sets of electrical resistivity vs. tempering-time curves are shown in Figs. 2-4. The curves for the two other very low-carbon alloys (Table I) are similar to those of Fig. 2; the curves for all other alloys have the same features as in Figs. 3 and 4.

The resistivity changes on aging the latter group of alloys can be divided into three regimes as illustrated schematically in Fig. 5: Regime I, an initial drop in resistivity; Regime II, an increase to a peak and a subsequent decrease; and Regime III, a continuation of the decrease at a slower rate to the fully-tempered plateau value. The three very low-carbon alloys do not exhibit the resistivity changes described above. The magnitudes of the initial (virgin) resistivity (Fig. 6) and the height of the resistivity peak (Fig. 7) increase linearly with the carbon content over the range of compositions studied. Likewise, the magnitude of the total decrease in resistivity occurring when the martensites are tempered at the higher temperatures for long times also increases with carbon content.

The x-ray diffraction measurements showed that all of the alloys with subambient M_s temperatures formed martensites which are initially body-centered tetragonal. The tetragonality ratio (c/a) increases in proportion to carbon content in agreement with previous observations[18-22]. Upon aging, new (002) diffraction spots appear, corresponding to a low-tetragonal martensite with c/a = 1.005. With continued aging, the new spots become more intense, while the initial, virgin martensite spots decrease in intensity. The time required for the completion of this change varies from several weeks at room temperature to a few minutes at 100°C. These findings are consistent with detailed observations on higher-carbon alloys[12,13].

The activation energies for the changes responsible for the above x-ray observations were estimated in the following way: By visual inspection of the x-ray films, the aging times necessary to attain equal intensities of the two sets of (002) spots, as well as the times for complete disappearance of the original (002) spots, were determined. From plots of log time vs. the reciprocal of the absolute aging temperature, the activation energies thus obtained lie close to 92 k joules (22 k cal) per mole for the half-way mark and 100 k joules (24 k cal) per mole for the complete transition from the high-tetragonality virgin martensite to the low-tetragonality aged martensite. These values are averages over all the alloys on which these x-ray diffraction measurements could be performed, and have an uncertainty of about 4 k joules (1 k cal) per mole.

Although the martensitic morpohologies vary with increasing carbon content from laths to mixed to plates in these Fe-Ni-C alloys, the microstructural changes observed on tempering are qualitatively the same for all alloys. Therefore, electron micrographs from the 0.4 C-13 Ni and 0.4 C-21 Ni alloys, which form plate martensites are presented here as representative. The microstructures of samples which had undergone room-temperature aging are quite similar to those found after aging at 100°C for one hour (Figs. 8 and 9). However, as mentioned previously, the preparation of metallographic specimens required considerable exposure to room temperature, and so it is to be expected that the microstructures of the "unaged" and 100°C/1 hour specimens will look much the same. Two striking metallographic features are the granular appearance or "salt-and-pepper" contrast seen in some areas, while

in others, there is a fine cross-hatched pattern reminiscent of the tweed structure attributed to pre-precipitation clusters of solute atoms in some alloy systems [33-34].

Tempering for one hour at 150°C and above results in the precipitation of carbides and progressive recovery of the martensitic substructure. After tempering at 150°C, bright-field evidence (Fig. 10) of ε-carbide* (first stage of tempering) is found. However, we were not able to detect carbide precipitation by electron diffraction on tempering below 200°C. Strain-constrast effects indicative of coherency are visible at this stage of precipitation. A fairly uniform distribution of ε-carbide is seen on tempering at 200°C (Fig. 11); cementite (third stage of tempering) appears on tempering at 300°C (Fig. 12). The cementite is less evenly distributed than the ε-carbide, tending to form preferentially at twin interfaces, lath boundaries, or along the center of larger laths as an apparent "midrib." Patches exhibiting the aforementioned salt-and-pepper contrast are still visible after the beginning of carbide precipitation. However, the granularity becomes much coarser and less extensive. On the other hand, the cross-hatched contrast disappears with the onset of precipitation. Tempering at 400°C results in substantial recovery of the substructure, with individual dislocations clearly resolvable for the first time. The salt-and-pepper contrast, which we associate with high dislocation densities, is largely absent at this stage.

4. Discussion of Results

The main thrust of this paper lies in the electrical resistivity measurements which provide a kinetic framework for interpreting the results. This approach lends itself to the use of virgin martensites as the starting state for aging and tempering studies, and also permits well-controlled aging experiments at subambient temperatures.

---

* For the purpose of this discussion, we are referring to this first carbide as ε, recognizing that its structure may, in fact, be orthorhombic (η-carbide)[32] rather than hexagonal close-packed.

4.1 Significance of Resistivity Changes

During the aging of martensite, we have observed several types of resistivity changes, and in order to understand their causes some general interpretation of resistivity changes is necessary. Basinski et al.[23] have explained the effect of dislocations on the resistivity of iron by considering the mean-square static displacements of iron atoms produced by the dislocation strain fields. In an analogous manner, Hoffman [24] compared the mean-square static displacements caused by interstitial atoms with those displacements arising from thermal effects, and then showed that iron lattice distortions could account for almost all of the resistivity increase due to the addition of carbon. Hence, in this work we adopt the following interpretation: Changes in martensite resistivity are assumed to arise from mechanisms which change the mean-square static displacements, $\overline{\mu^2}$, of the Fe-atom (or, here, Fe-Ni atom) lattice. If $\overline{\mu^2}$ decreases, as by the removal of solute carbon or by the annealing out of defects, the resistivity also decreases, and conversely.

The initial resistivities of the martensites in this study increase linearly with carbon content (Fig. 6), in line with previous findings [7]. From this relationship, the indications are that all the carbon atoms are initially in solution in the martensite before any aging. This conclusion is reinforced by the fact that, with the exception of the nil-carbon alloys (which exhibit only small resistivity changes as a result of aging, Fig. 2) the resistivity response to aging and tempering of all the martensites is qualitatively the same and in proportion to the carbon content.

4.2 Regime I: Initial Resistivity Decrease

The initial resitivity drop is a relatively rapid phenomenon, being complete (to the minimum value reached) within a matter of minutes even at $-95^{\circ}C$. The existence of Regime I is a good indication that the martensite is in its virgin condition at the start of testing, since inadvertent aging due to auto-tempering or unintentional warming will obscure the initial resistivity decrease before the beginning of the test run.

The time-temperature characteristics of the resistivity decrease in Regime I are consistent with the isothermal transformation of small amounts of

retained austenite. However, the possibility of a very subtle relaxation taking place within the virgin martensite itself is not ruled out. Recent x-ray diffraction observations indicate a slight reduction in tetragonality during the warming of virgin martensite from the liquid nitrogen temperature to $-50^{\circ}C$[40]. This change has been interpreted to be caused by small movements of some atoms trapped in very high-energy energy positions as a result of low-temperature martensitic transformation[41]. These are comparatively minor structural changes in the present context.

4.3 Regime II: Resistivity Peak and Subsequent Decline

Within the time span of our experiments, resistivity increases are noted in specimens aged at temperatures between -40 and + $100^{\circ}C$, with actual peaks observed on aging between 0 and $70^{\circ}C$. Aging below $0^{\circ}C$ produces an increase in resistivity after long times, while specimens aged at $100^{\circ}C$ and above apparently pass the peak in less than the minimum aging treatment of 15 seconds. The height of the peak, $\Delta\rho_{II}$, increases linearly with carbon content of the martensite (Fig. 7) and does not seem to vary in a systematic way with aging temperature.

The above kinetics are characteristic of a thermally activated process. Activation energies for Regime II were determined by noting the log of the time for a given extent of the process and plotting this vs. 1/T. It was assumed that the attainment of equal fractions of the total peak height (or decline in resistivity after reaching the maximum value) corresponds to equivalent fractions of the total process, independent of temperature. The activation energies thus obtained vary from 75 $\pm$ 4 k joules (18 $\pm$ 1 k cal) per mole during early stages of the resistivity increase, to 88 k joules (21 k cal) at the summit of the peak, up to 100 k joules (24 k cal) per mole during the initial stages of the subsequent decline in resistivity. These values and trends are found to be the same for all the alloys.

The emergence of a low-tetragonality martensite and the disappearance of the as-quenched tetragonal martensite (as revealed by the x-ray diffraction experiments) occur within the same time-temperature range as Regime II, and

the activation energies and trends evaluated by both types of measurement agree closely. These values are also in line with the experimentally determined activation energies of 75.7 to 102.9 k joules (18.1 to 24.6 k cal) per mole for the diffusion of carbon in α-Fe [26] and with calculations by Hillert [27] for the diffusion of carbon in martensite. Accordingly, we conclude that both the changes in tetragonality and the resistivity peak are manifestations of the same carbon-dependent process.

Along these lines, it was previously suggested that the resistivity peak is due to an early stage of ϵ-carbide precipitation [21,28]. However, the present results and those of Hoffman [25] indicate that ϵ-carbide is not formed until later in the aging process, at the time-temperature combinations corresponding to the onset of Regime III.

Although carbide precipitation is not observed until later in the tempering sequence, there have been numerous references to the formation of carbon clusters in the time-temperature range of Regime II. The latter experiments were conducted on high-carbon (> 1%) martensites using x-ray diffraction [12,13], field ion microscopy [17], electron microscopy [14-16,29,30] and Mössbauer spectroscopy [8-11]. While the present results on lower carbon alloys do not reveal the subtleties seen in some of the above investigations, nevertheless they are consistent. In addition, Hoffman [24] has developed a theory, based on increasing mean-square displacements of the iron atoms, to account for the resistivity increase caused by carbon-atom clustering at an early stage. It is quite evident, then, that the resistivity changes of Regime II are due to the formation of carbon-rich clusters.

The process of carbon-cluster formation during the aging of martensite may proceed in the following way: Virgin martensite inherits a nonrandom distribution of carbon atoms from the parent austenite such that the carbons tend to be as far apart from one another as possible [10]. Upon aging, carbon atoms jump interstitially from site to site in the body-centered-tetragonal martensite to form clusters of two to four carbons [12]. During this process, the carbon atoms occupy octahedral sites in one of the three possible sets, such occupancy being inherited from the austenite. The driving force for the

grouping of carbons in this manner is a reduction in the lattice-distortion strain energy caused by the interstitial atoms [24]. Johnson [39] has calculated the binding energy for several types of carbon pairs to be 0.10 ± 0.01 ev. One could expect that the binding energy of a third or fourth carbon atom would be somewhat similar. These small clusters are considered to be generally distributed throughout the martensitic lattice, and since the carbon atoms are still in interstitial solution and on the original set of octahedral sites, the martensite is still tetragonal. As the small clusters continue to develop, some grow at the expense of others, i.e., a form of coalescence takes place. It is during the early stages of this process that increases in the mean-square displacement of the iron atoms leads to the resistivity peak. The coarsening of the clusters entails the debonding of carbon atoms from smaller clusters, and so the activation energy for this type of carbon jump is larger than that for normal lattice jumps since the binding energy to the cluster must be overcome. Hence, debonding will then become the rate-determining step. The 0.1 ev di-carbon binding energy corresponds to an activation energy increase of 9.6 k joules (2.3 k cal) per mole and, in approximate terms, accounts for the observed gradual increase in activation energy in Regime II as determined by the resistivity and x-ray measurements. With further cluster-coarsening, regions of the martensitic lattice become depleted in carbon, thereby resulting in the emergence of low-tetragonality martensite as observed by x-ray diffraction. At this stage, the larger clusters are visualized to behave more like domains or zones. Although the local distortions near the clusters are still large, the mean free path between them has increased to the point that the bulk of the lattice distortion has decreased and so the resistivity begins to decrease, still within Regime II. The final composition of the large clusters appears to approximate Fe_4C [10,11,14]. Chen and Winchell [13] have detected a range of axial ratios - from just below unity to just above - at this point, and attributed these effects to coherency distortions in the carbon-depleted regions.

4.4 Regime III: Continued Resistivity Decrease

Aging at temperatures above 100°C, or beyond the peak at lower temperatures, is accompanied by a progressive decrease in resistivity with aging time. From electron microscopy, it is clear that during this time-temperature span ε-carbide is formed and is, in turn, superseded by the precipitation of

cementite (Fe_3C) at higher temperatures or longer tempering times. Moreover, at higher temperatures, recovery and eventually recrystallization occur. By taking the resistivity plateau reached after long tempering times at 300° or 350°C to represent the completion of carbide precipitation, we can estimate the activation energy of the process at stages along the resistivity decline, adopting a method suggested by Hillert [27]. The values thus obtained increase from 100 k joules (24 k cal) per mole to about 146 k joules (35 k cal) per mole, Fig. 13. The lower value persists through approximately 40% of the decline, which is about the location of a change in slope of the resistivity vs. log time curves; this point is taken as the demarcation between Regimes II and III. The increasing activation energy after about 40% of the overall resistivity decline suggests that two structural changes are occurring simultaneously: cluster growth and coalescence with $Q \simeq 100$ k joules per mole and a second process with an activation energy value of about 146 k joules per mole. The intermediate activation energies can then be interpreted as average values reflecting an overlap of the two processes. The onset of the increase in observed activation energy (the beginning of Regime III) corresponds to the time-temperature range in which ε-carbides are just observed by electron microscopy. Hence, we conclude that the activation energy of 146 k joules per mole represents the rate-determining step in this precipitation reaction. This value is, of course, much too high for carbon diffusion and too low for lattice self-diffusion of iron [26]. However, it does lie in the range determined for the diffusion of iron atoms along dislocation pipes [31].

At this point, it is worth considering whether ε-carbide nucleates and grows separately from, and at the expense of, the carbon-rich clusters or whether ε-carbide forms directly from the clusters when they reach some critical size. Such clusters, perhaps having the Fe_4C composition as has been proposed [9-11,14-16], may then squeeze out iron atoms along dislocation paths in order to lower the free energy by relieving coherency strain energy. Loss of iron atoms would then allow the local lattice of the cluster to relax into the hcp (or orthothombic [32]) ε-carbide structure. While no direct evidence is available for this idea yet, support can be drawn from several sources. Electron microscopy shows that ε-carbide seems to emerge from the cross hatched strain contrast as the aging temperature is increased. This is similar to the formation

of precipitates from the "tweed" structures seen in Al-Cu and other systems[33–35]. Also, the above outlined clustering/precipitation process would be similar to that observed by Jack [36] in the Fe-N system.

The final step in the carbide-precipitation sequence is the formation of cementite, which nucleates and grows independently and at the expense of the ε-carbide at the higher tempering temperatures. At the stage where cementite is forming (after approximately 70% of the resistivity decrease has taken place) the activation energy is about 146 k joules (35 k cal) per mole. This suggests that the rate-controlling steps for both ε-carbide and cementite formation are the same, namely diffusion of iron and substitutional atoms away from the growing carbide particles along dislocation paths. During the initial stages of cementite precipitation, ε-carbide may still be forming before it subsequently redissolves in favor of the cementite. Accordingly, in these iron-nickel-carbon alloys, there is an overlap between the two precipitation reactions. In other words, the well-known first and third stages of tempering are not well separated here as in other steels [18,19].

4.5 Substructural Effects on Martensite Aging

Previous investigations [3,7] have indicated that martensitic morphology exerts a substantial influence on the tempering behavior, e.g., in the segregation of carbon atoms to dislocation sites and/or lath boundaries. Such segregation has been considered to involve a large fraction of the carbon atoms present in low-carbon alloys, and this conclusion is supported by calculations[37] showing that more than 0.1 weight percent carbon may be accommodated by dislocations in the densitites typical of lath martensites. The present results, however, do not reveal any differences in aging behavior among the different martensitic morphologies encountered here. All of the carbon-containing martensites exhibit the same kinds of aging regimes, and both the magnitudes and kinetics of such changes depend explicitly on the carbon content rather than on the morphology. This means that the observed trends vary smoothly with carbon content even when the morphology changes. Furthermore, the detection of a resistivity peak in all such cases signifies that clustering is the dominant process which occurs during the aging of these freshly-quenched ($M_s > RT$) or virgin martensites ($M_s < RT$) prior to carbide formation. Segregation of carbon atoms to dislocations or cell boundaries should be reflected in a decrease of

resistivity. On the other hand, these observations cannot be taken to rule out such segregation processes; it may be that (a) they are dominated by cluster formation in influencing the resistivity changes, or (b) the dislocation densities of all the martensites studied here may be so high (even the twinned martensites contained densely dislocated regions as evidenced by the granular or "salt and pepper" contrast previously noted) that the morphological variations behave more-or-less alike as far as aging is concerned. Previous results tending to give evidence of carbon segregation to structural defects have been obtained on Fe-C alloys with relatively high M_s temperatures. The resulting auto-tempering undoubtedly obscures the clustering regime that prevails during the aging of low-M_s (freshly-quenched or virgin) martensites.

The re-solution of carbides as a result of strain tempering [37,38] has also been interpreted as evidence for the dislocation trapping of carbon atoms as a pre-carbide step in the tempering sequence. These effects are not inconsistent with the present finding that clustering, rather than carbon migration to defects, is the dominant phenomenon in the aging of undeformed martensites. It is conceivable that dislocations newly generated by plastic deformation are more potent as carbon sinks than are the dislocations arising from the martensitic transformation itself.

5. Summary

The results of the present study on Fe-Ni-C martensites, correlated with other observations, have led to a refined description of the phenomena which take place as virgin martensite is aged or tempered. The changes observed are both temperature- and time-dependent. At subambient temperatures, the first change detected is attributed to isothermal conversion of a small amount of retained austenite, or slight relaxations in the martensite, but this is not a significant part of the martensite-aging process. The remainder of the changes are martensite-related and diffusion-controlled. Aging from subzero temperatures up to about 70°C is accompanied by the formation of carbon-rich clusters which, at first, have only a few carbon atoms per cluster. These small clusters coarsen to become larger domains, probably reaching a composition of Fe_4C. This process is controlled by carbon-atom diffusion and depletes the martensite lattice of carbon, with the attendant emergence of low-tetragonal martensite.

Tempering at higher temperatures also results in the formation of ε-carbide and eventually cementite. There is some reason to believe that ε-carbide forms directly from the carbon clusters. The two carbide precipitations, corresponding to the usual first and third stages of tempering, overlap and their kinetics appear to be controlled by iron and substitutional atom diffusion along dislocation paths.

Figure 14 summarizes the temperature and time ranges in which each of the above changes is observed. Martensitic morphology is found to have no measurable effect on the aging and tempering behavior under the conditions of these studies.

Acknowledgments

The authors wish to express their thanks to the Office of Naval Research for the sponsorship of research on tempering at MIT over many years, presently under Contract No. N00014-81-K-0013. AMS is grateful to the Climax Molybdenum Company of Michigan for a fellowship grant while he was a graduate student at MIT. Similarly, GTE is grateful to the Bethlehem Steel Corporation for a research grant and to the National Aeronautics and Space Administration for the award of a Traineeship while he was a graduate student at MIT. It is also a pleasure to acknowledge the valuable participation of Marguerite Meyer and Miriam Rich at various stages of this work. The iron-nickel-carbon alloys for this investigation were kindly furnished by the United States Steel Corporation.

Appendix

Conversion of Resistance to Resistivity and Correction for the Presence of Retained Austenite

As noted in the text, the raw data for this work were obtained from resistance measurements on two-phase (martensite + austenite) specimens at liquid-nitrogen temperature. To convert these resistances to resistivity values corresponding to 100% martensite, a three-step process was used.

First, the resistance measurements of the two-phase specimens were converted to resistivities by taking account of the specimen geometry:

$$\rho\ (\gamma + M) = R\ (\gamma + M)\ \cdot \frac{A}{L} \qquad (A.1)$$

where ρ = resistivity in microhm-cm,
R = resistance in microhm,
A = specimen cross-sectional area in cm^2,
L = specimen length in cm,

and the letters γ and M refer to the austenite and martensite phases, respectively.

For any one alloy, the initial (as-quenched) specimen resistivities thus obtained varied considerably due to inaccuracies in measurement of specimen geometry. In particular, the swaging operation yielded wire specimens of non-uniform cross section. To compensate for these geometrical errors, a normalization factor, F, was established for each specimen, i, as:

$$F_i = \frac{\overline{\rho_o}}{\rho_{o_i}} \qquad (A.2)$$

where $\overline{\rho_o}$ is the average initial resistivity of all the specimens of a given alloy, and ρ_{o_i} is the initial resistivity of the ith specimen of that alloy. Thus, the second step of the conversion was to multiply all the resistivity data for a given

specimen by the normalization factor for that specimen, thereby obtaining resistivity vs. time curves normalized to a common initial resistivity value.

The third step in the conversion was to correct for the retained austenite present in those alloys forming martensites of mixed and plate morphologies. In general, the resistivity of a two-phase mixture will depend on the resistivities of the two phases (here ρ_γ and ρ_M), on the relative volume fractions (here V_γ and V_M), and on the distribution of the two phases. Two extremes in distribution can be considered. At one extreme, the phases may be imagined completely separated from one another, at opposite ends of the specimen. In such a case of two resistances in series, the resistivities add, giving:

$$\rho_{\gamma+M} = \rho_M V_M + \rho_\gamma (1-V_M) \qquad (A.3)$$

At the other extreme, the phases are again completely separated, but with each phase running continuously from one of end of the specimen to the other. In this case of two resistances in parallel, the conductivities are additive:

$$\rho_{\gamma+M} = \left[\frac{1}{\rho_M} \cdot V_M + \frac{1}{\rho_\gamma} \cdot (1-V_M)\right]^{-1} \qquad (A.4)$$

The most general case, of course, lies somewhere between these two extremes, and can be written:

$$\rho_{\gamma+M} = Z\left[\frac{V_M}{\rho_M} + \frac{(1-V_M)}{\rho_\gamma}\right]^{-1} + (1-Z)\left[\rho_M V_M + \rho_\gamma (1-V_M)\right] \qquad (A.5)$$

where Z represents the "fractional parallel character" of the two-phase mixture, and (1-Z) the "fractional series character." The other quantities are as defined before. This formulation was apparently first used by Hoffman[25] who, for an Fe-23% Ni-0.4%C alloy, empirically determined Z=0.65 over a wide range of tempering treatments for two-phase martensite + austenite mixtures. Because our alloys were so similar to Hoffman's, the value Z = 0.65 was also adopted for the present work.

In Equation A.5, $\rho_{\gamma+M}$ and V_M are both measured quantities. ρ_γ at -196^oC is obtained by converting the room temperature resistivity of fully

austenitic specimens via the known temperature dependence of ρ_γ for a very similar alloy[25].

Thus, by means of Equation A.5, the desired values of ρ_M can be derived. This, of course, assumes that ρ_γ changes only insignificantly during the course of tempering the two-phase specimens. Our work on fully austenitic specimens of the alloys used here verify this assumption since no significant changes in resistivity are observed after tempering for up to 1000 minutes at up to 300°C.

References

1. L. Kaufman and M. Cohen: "Thermodynamics and Kinetics of Martensite Transformations," Progress in Metal Physics 7 (1958) pp. 165-246.

2. D. P. Dunne and C. M. Wayman: "The Crystallography of Ferrous Martensites," Met. Trans. 2 (1971) pp. 2327-2341.

3. G. R. Speich and W. C. Leslie: "Tempering of Steel," Met. Trans. 3 (1972) pp. 1043-1054.

4. Y. Imai: "Phases in Quenched and Tempered Steels," Trans. Japan Inst. Met. 16 (1975) pp. 721-734.

5. O. Johari and G. Thomas: "Factors Determining Twinning in Martensite," Acta Met. 13 (1965) pp. 1211-1212.

6. V. I. Izotov and F. A. Khandarov: "A Classification of Martensite Structures in Iron Alloys," Phys. Met. Metallog. 34 No. 2 (1972) pp. 101-106.

7. G. R. Speich: "Tempering of Low-Carbon Martensite," Trans. AIME 245 (1969) pp. 2553-2564.

8. J. R. Genin and P. A. Flinn: "Mossbauer Effect Study of the Clustering of Carbon Atoms During the Room Temperature Aging of Iron-Carbon Martensite," Trans. AIME 242 (1968) pp. 1419-1430.

9. W. K. Choo and R. Kaplow: "Mössbauer Measurements on the Aging of Iron-Carbon Martensite," Acta Met. 21 (1973) pp. 725-732.

10. N. DeCristofaro and R. Kaplow: "Interstitial Atom Configurations in Stable and Metastable Fe-N and Fe-C Solid Solutions," Met. Trans. A 8A (1977) pp. 35-44.

11. N. DeCristofaro, R. Kaplow and W. S. Owen: "The Kinetics of Carbon Clustering in Martensite," Met. Trans. A 9A (1978) pp. 821-825.

12. P. C. Chen, B. O. Hall and P. G. Winchell: "Atomic Displacements Due to C in Fe-Ni-C Martensite," Met. Trans. A 11A (1980) pp. 1323-1331.

13. P. C. Chen and P. G. Winchell: "Martensite Lattice Changes During Tempering," Met. Trans. A 11A (1980) pp. 1333-1339.

14. V. I. Izotov and L. M. Utevskiy: "Structure of the Martensite Crystals of High-Carbon Steel," Phys. Met. Metallog. 25 No. 1 (1968) pp. 86-96.

15. A. K. Sachdev: "The Substructure and Aging of High-Carbon Ferrous Martensites," PhD Thesis, MIT (1977).

16. S. Nagakura and M. Toyoshima: "Crystal Structure and Morphology of the Ordered Phase in Iron-Carbon Martensite," Trans. SIM 20 (1979) pp. 100-110.

17. P. A. Beaven, M. K. Miller and G. D. W. Smith: "Carbon Atom Redistribution During the Aging and Early Stages of Tempering of Ferrous Martensites," Proc. Int. Conf. on Martensitic Transformations, Cambridge, MA (1979) pp. 559-563.

18. C. S. Roberts, B. L. Averbach and M. Cohen: " The First Stage of Tempering," Trans. ASM 45 (1953) pp. 576-604.

19. F. E. Werner, B. L. Averbach, and M. Cohen: "Tempering of Martensite Crystals," Trans. ASM 49 (1957) pp. 823-41.

20. P. G. Winchell: The Structure and Mechanical Properties of Iron-Nickel-Carbon Martensites, PhD Thesis, MIT (1958).

21. P. G. Winchell and M. Cohen: "The Strength of Martensite," Trans. ASM 55 (1962) pp. 347-361.

22. A. K. Sachdev and P. G. Winchell: "The Non-Cubic Lattice of Rapidly Quenched Packet Martensite," Met. Trans. A 6A (1975) pp. 59-63.

23. Z. S. Basinski, J. S. Dugdale and A. Howie: "The Electrical Resistivity of Dislocations," Phil. Mag. 8 (1963) pp. 1989-1997.

24. D. W. Hoffman and Morris Cohen: "Static Displacements and the Electrical Resistivity of Interstitial Alloys," Acta Met. 21 (1973) pp. 1215-1223.

25. D. W. Hoffman: Ausform-Strengthening of Iron-Nickel-Carbon Martensite," PhD Thesis, MIT (1966).

26. Y. Adda and J. Philibert: La Diffusion Trans les Solides, Presses Universitaires de France, Paris (1966).

27. M. Hillert: "The Kinetics of the First Stage of Tempering," Acta Met. 7 (1959) pp. 653-658.

28. H. W. King and S. G. Glover: "A Resistometric Study of the First Stage of Tempering in Plain Carbon Steels," JISI 193 (1959) pp. 123-132.

29. A. G. Khachaturyan and J. A. Orrisimova: "Theory of Diffuse Electron Scattering Due to Short-Range Order in Ferrocarbon Martensite," Phys. Met. Metallog. 26 No. 6 (1969) pp. 12-19.

30. G. V. Kurdyumov and A. G. Khachaturyan: "Phenomena of Carbon Atom Redistribution in Martensite," Met. Trans. 3 (1972) pp. 1069-1076.

31. M. Cohen: "Self-Diffusion During Plastic deformation," Trnas. Japan Inst. Met. 11 No. 3 (1970) pp. 145-151.

32. Y. Hirotsu and S. Nakagura: "Crystal Structure and Morphology of the Carbide Precipitated from Martensitic High Carbon Steel During the First Stage of Tempering," Acta Met. 20 (1972) pp. 645-655.

33. L. E. Tanner: "Diffraction Contrast from Elastic Shear Strains Due to Coherent Phases," Phil. Mag. 14 (1966) pp. 111-130.

34. P. J. Fillingham, H. J. Leamy and L. E. Tanner: "Simulation of Electron Transmission Images of Crystals Containing Random and Periodic Arrays of Coherency Strain Centers," Electron Microscopy and Structure of Materials, G. Thomas, ed. Univ. of Calif. Press, Berkley (1972) pp. 163-172.

35. P. E. Champness and G. W. Lorimer: "Electron Microscopic Studies of Some Lunar and Terrestrial Pyroxenes," Electron Microscopy and Structure of Materials, G. Thomas, ed. Univ. of Calif. Press, Berkley (1972) pp. 1245-1255.

36. K. H. Jack: "The Occurrence and the Crystal Structure of α"-Iron Nitride; a New Type of Interstitial Alloy Formed During the Tempering of Nitrogen-Martensite," Proc. Ray. Soc. A208 (1951) pp. 216-224.

37. D. Kalish and M. Cohen: "Structural Changes and Strengthening in the Strain Tempering of Martensite," Material Science and Engineering 6 (1970) pp. 156-166.

38. G. T. Eldis and M. Cohen: to be published in this Symposium.

39. R. A. Johnson: "Calculation of the Energy and Migration Characteristics of Carbon in Martensite," Acta Met. 13 (1965) pp. 1259-1262.

40. M. Hayakawa, Y. Uemura and M. Oka: "Discussion of Atomic Displacements Due to C in FeNi C Martensite," Met. Trans. A, 12A (1981) pp. 1545-1547.

41. P. G. Winchell, P. C. Chen and B. O. Hall: Author's Reply (to Ref. 40) Met. Trans. A, 12A (1981) pp. 1547-1548.

TABLE I

Compositions of Alloys

Series	C (wt%)	Ni (wt%)	Est. M_S (^oC)	Martensite Morphology
	0.0033	18.3	250	Lath
	0.11	18.1	180	Lath
18 Nickel	0.40	18.3	20	Plate
	0.50	18.3	10	Plate
	0.62	18.4	-20	Plate
	0.0078	20.8	200	Lath
	0.10	20.8	130	Lath
	0.20	20.7	80	Mixed
21 Nickel	0.25	21.8	40	Mixed
	0.30	21.5	25	Plate
	0.35	21.6	5	Plate
	0.40	21.1	-7	Plate
	0.0078	24.6	110	Lath
	0.12	24.6	50	Lath
	0.14	24.7	35	Mixed
24 Nickel	0.19	25.5	10	Mixed
	0.26	23.9	-2	Plate
	0.24	25.5	-10	Plate
	0.28	25.2	-30	Plate

All alloys contained less than 0.003 w/o Si and less than 0.005 w/o Mn.

Figure Captions

Figure 1 The morphology and M_s temperatures of Fe-Ni-C martensites as a function of composition.

Figure 2 Resistivity (at -196°C) vs. aging time at various temperatures for lath martensite formed in an Fe-18Ni-0.0033C alloy.

Figure 3 Resisitivity (at -196°C) vs. aging time at various temperatures for lath martensite formed in an Fe-18Ni-0.11C alloy.

Figure 4 Resistivity (at -196°C) vs. aging time at various temperatures for plate martensite formed in an Fe-21Ni-0.40C alloy.

Figure 5 Schematic resistivity vs. aging time/temperature identifying the changes and regimes which occur during the aging and tempering of martensite.

Figure 6 Initial resistivities (measured at -196°C) of freshly quenched (M_s > RT) and virgin (M_s < RT) martensites as a function of alloy composition.

Figure 7 Height of the resistivity peak (measured at -196°C) in Regime II as a function of alloy composition.

Figure 8 Electron micrograph of martensite formed in an Fe-21Ni-0.40C alloy and exposed to ambient temperatures during specimen preparation. Note the granular appearance throughout the structure; in some area, there is a faint cross-hatched or tweed-like appearance (C).

Figure 9 Electron micrograph of martensite in an Fe-18Ni-0.40C alloy aged at 100°C for one hour. Substantial areas exhibiting the cross-hatched or tweed-like strain contrast effect (C) can be seen. Note also the fine twins (T) in plate martensite.

Figure 10 Electron micrograph of martensite in an Fe-18Ni-0.40C alloy tempered at 150°C for one hour. Arrays of very fine carbide particles can be seen in most areas, while in others particles too small to resolve individually apparently give rise to a strain-contrast effect (S). Martensitic twinning (T) is also shown.

Figure 11 Electron micrograph of martensite in an Fe-21Ni-0.40C alloy tempered at 200°C for one hour. Well-developed arrays of -carbide particles are present. Note areas of coarser granular strain contrast (G) compared to Fig. 8.

Figure 12 Electron micrograph of martensite in an Fe-21Ni-0.40C alloy tempered at 300°C for one hour. Large cementite particles are evident, as are areas of coarse granular strain contrast (G) attributable to dislocation tangles.

Figure 13 Activation energy vs. fraction of the total resistivity decrease in Regimes II and III for lath martensite (Fe-18Ni-0.11C) and plate martensite (Fe-24Ni-0.26C and Fe-21Ni-0.40C).

Figure 14 Schematic summary of structural changes during the aging and tempering of virgin martensites correlated with accompanying resistivity changes.

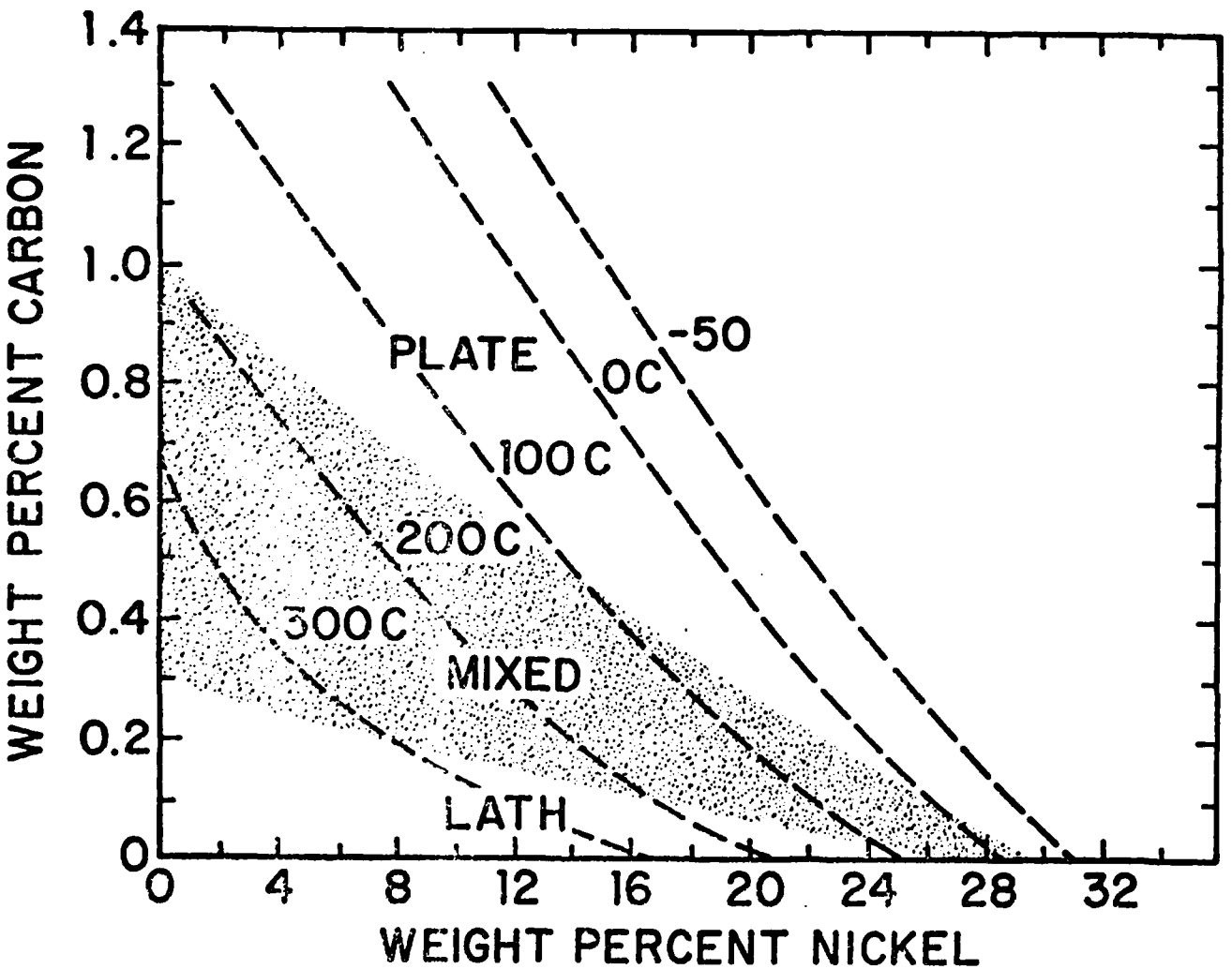

Fig. 1: The morphology and Ms temperatures of Fe-Ni-C martensites as a function of composition.

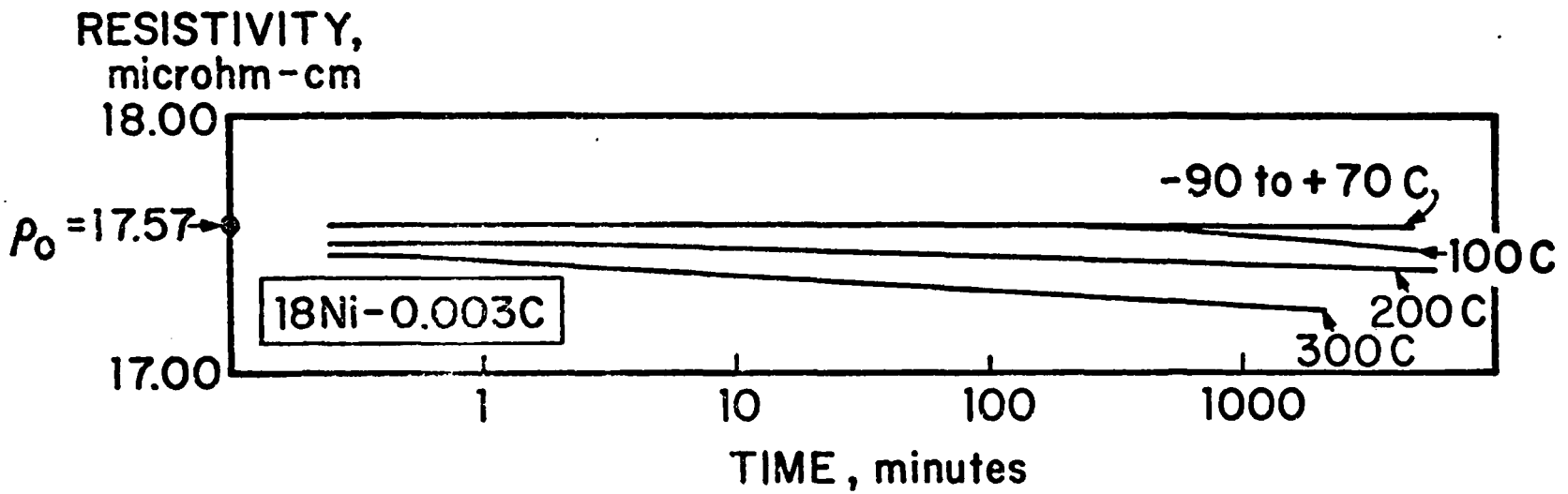

Fig. 2: Resistivity (at -196°C) vs. aging time at various temperatures for lath martensite formed in an Fe-18Ni-0.0033C alloy.

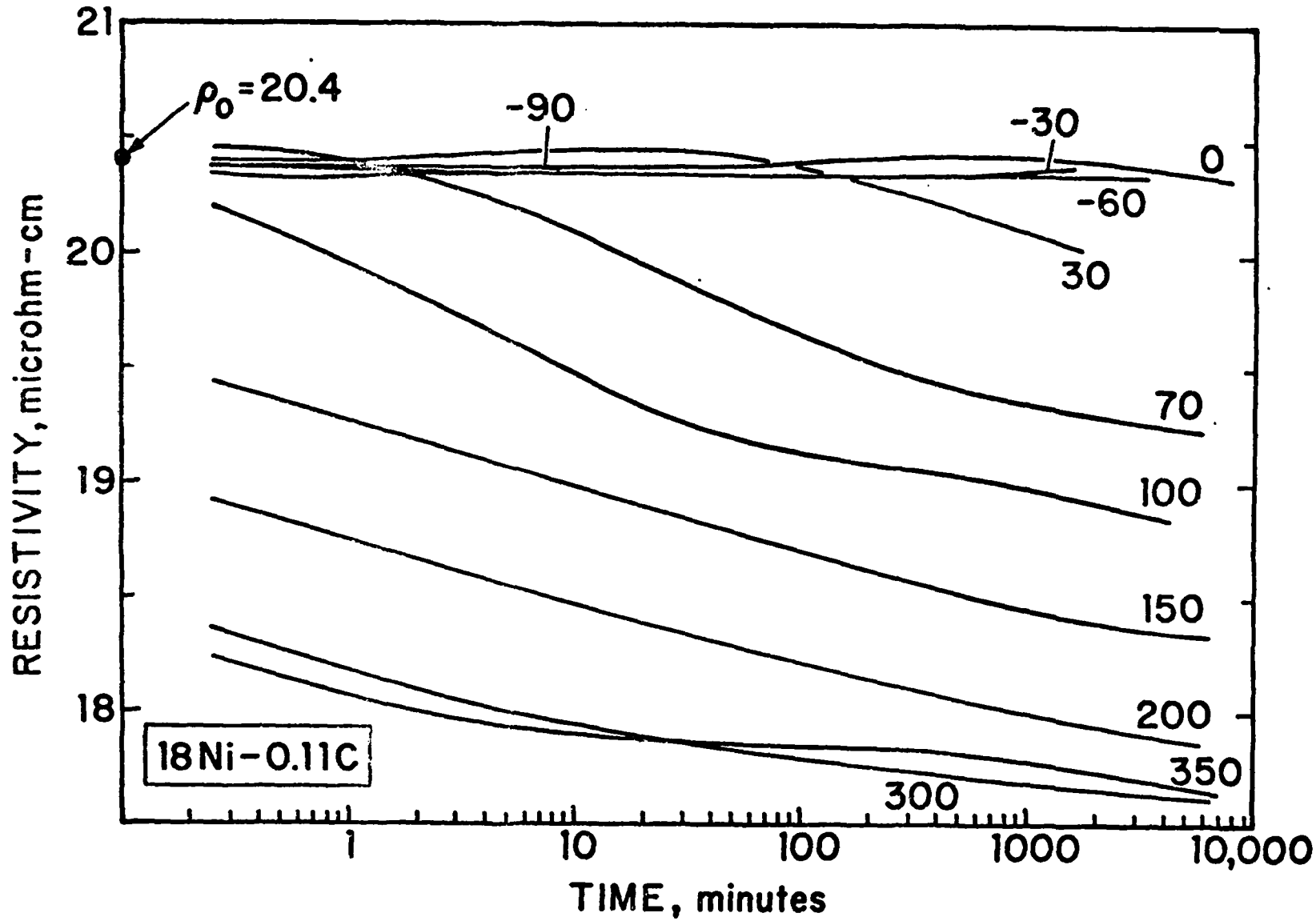

Fig. 3: Resistivity (at -196°C) vs. aging time at various temperatures for lath martensite formed in an Fe-18Ni-0.11C alloy.

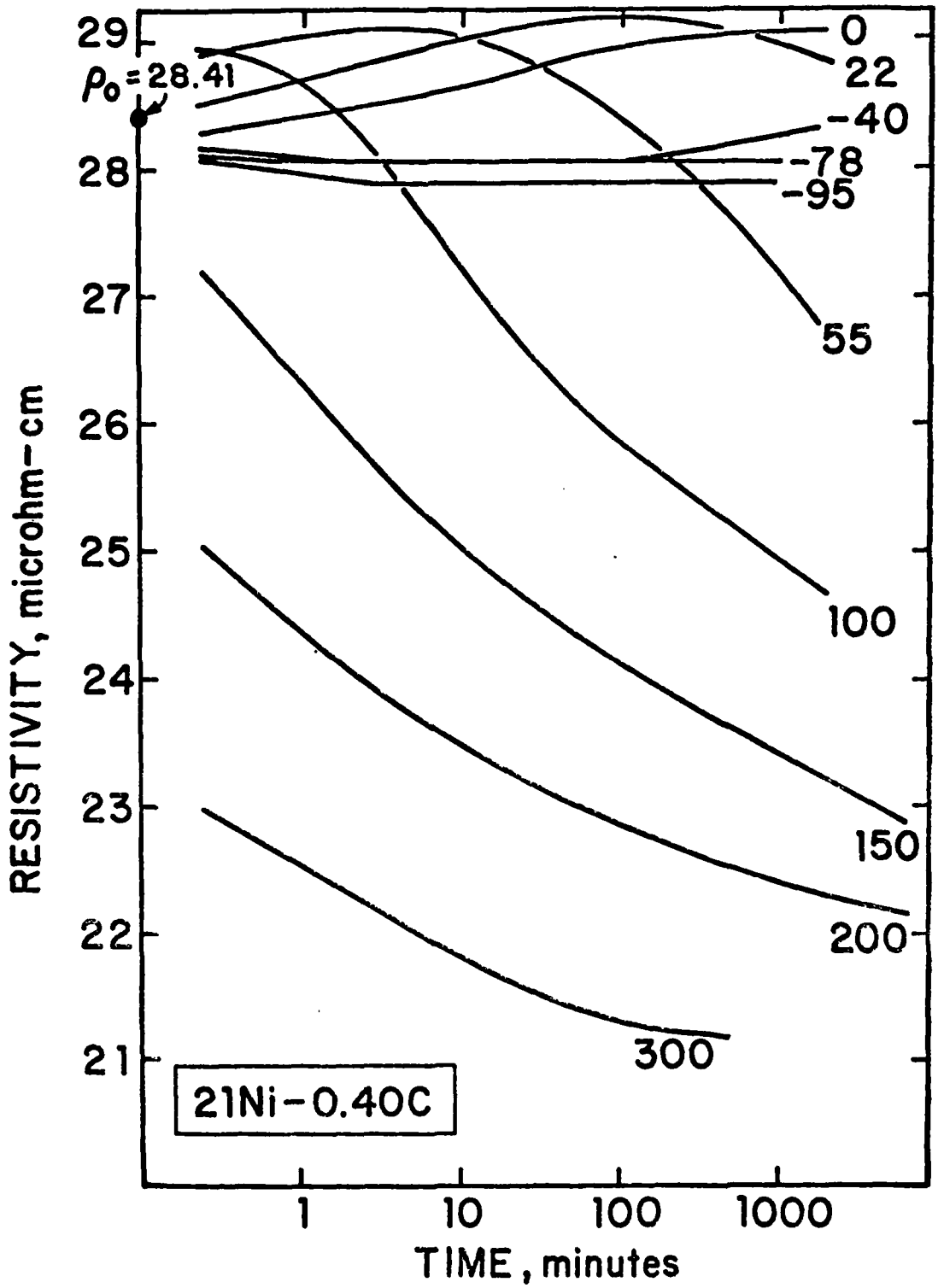

Fig. 4: Resistivity (at -196°C) vs. aging time at various temperatures for plate martensite formed in an Fe-21Ni-0.40C alloy.

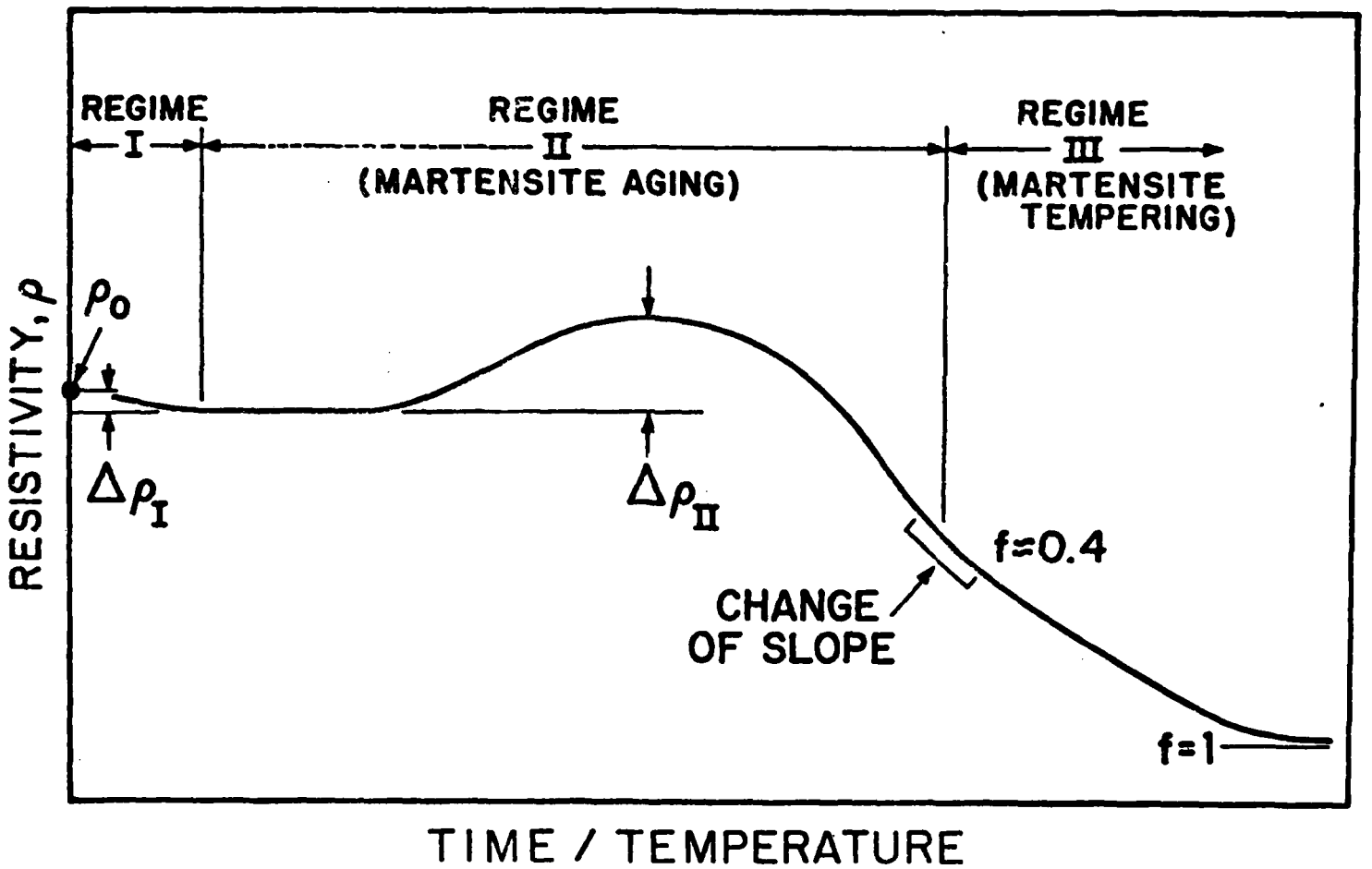

Fig. 5: Schematic resistivity vs. aging time/temperature curve identifying the changes and regimes which occur during the aging and tempering of martensite.

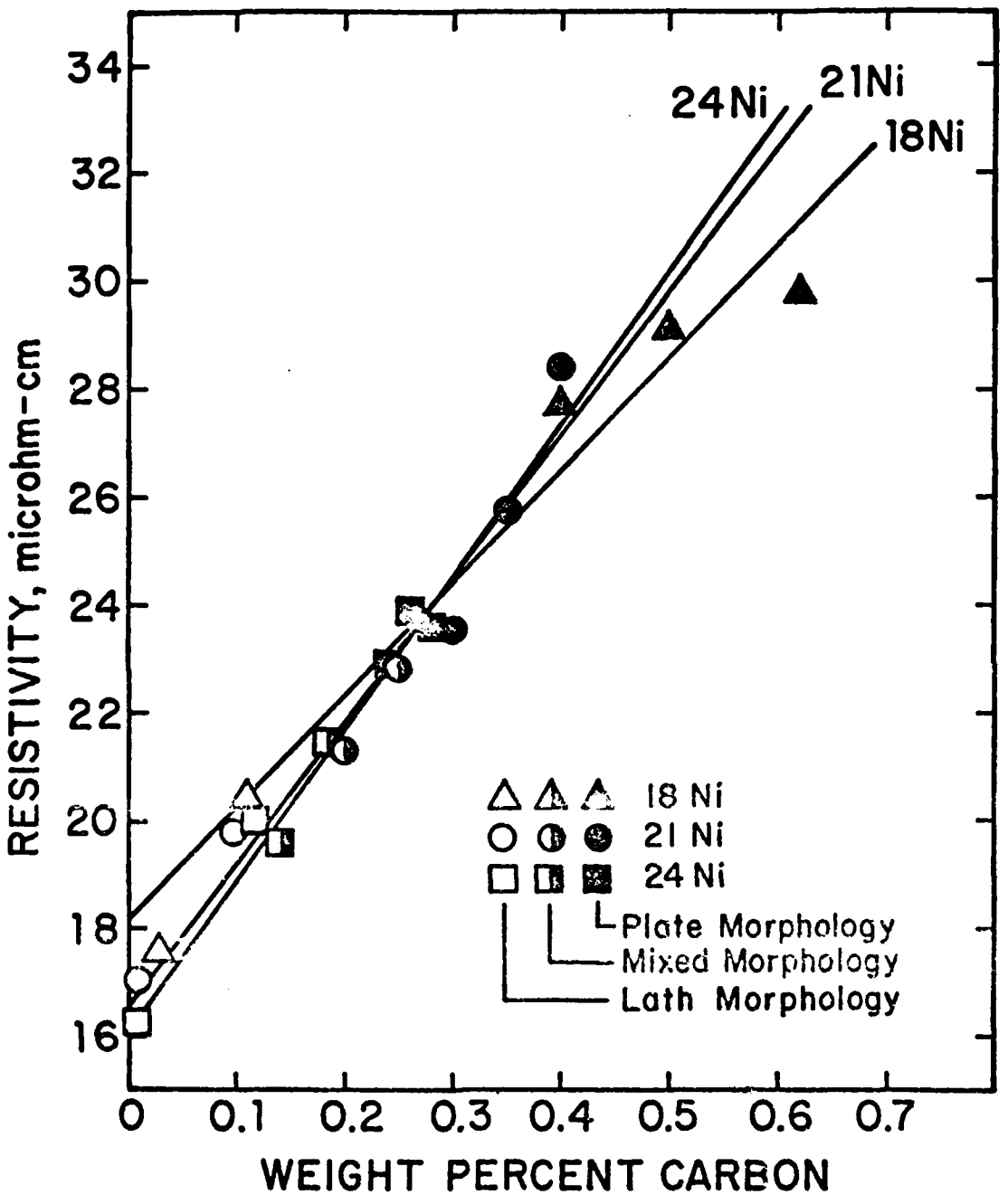

Fig. 6: Initial resistivities (measured at -196°C) of freshly quenched (Ms > RT) and virgin (Ms < RT) martensites as a function of alloy composition.

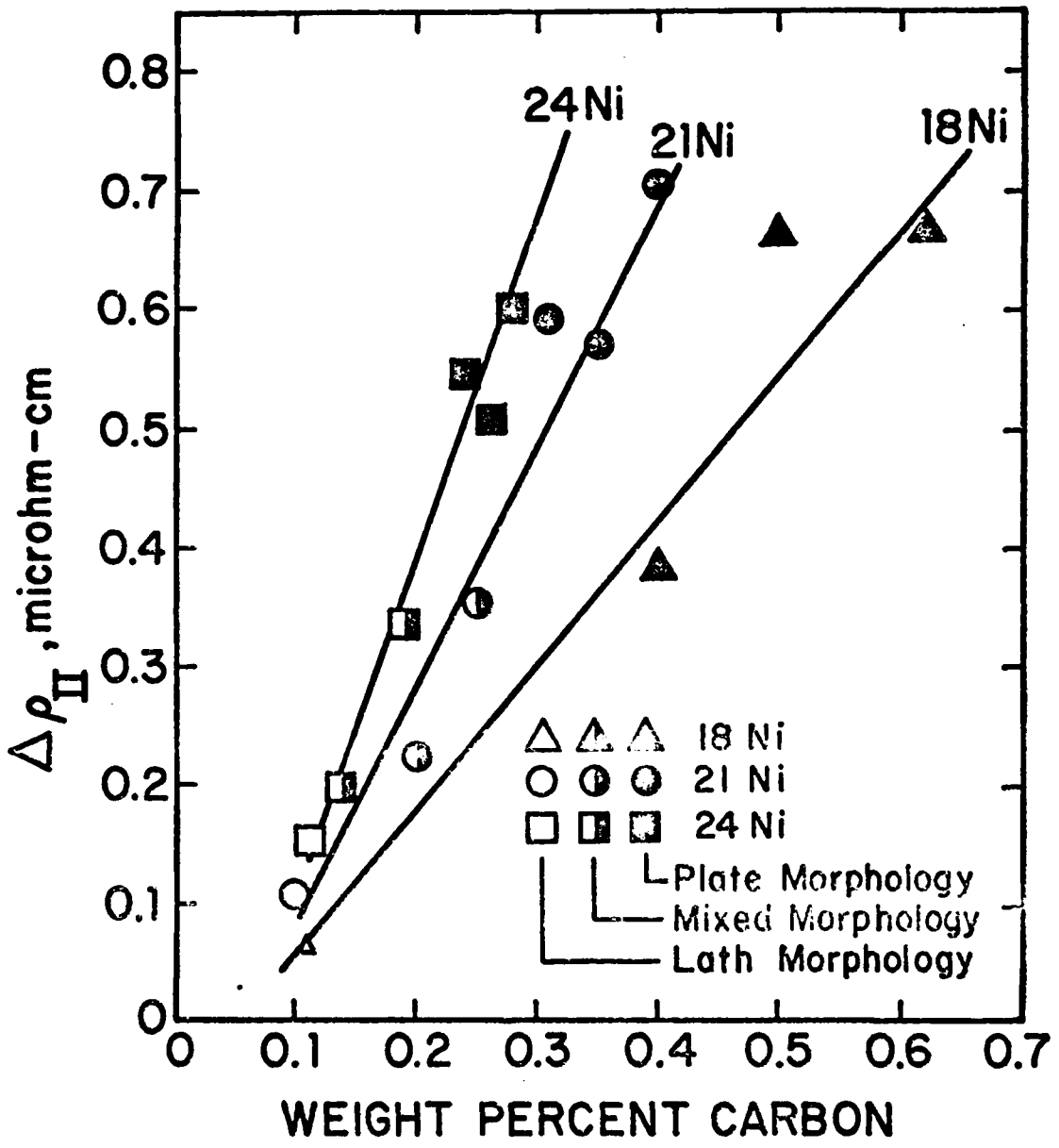

Fig. 7: Height of the resistivity peak (measured at -196°C) in Regime II as a function of alloy composition.

Fig. 8: Electron micrograph of martensite formed in an Fe-21Ni-0.40C alloy and exposed to ambient temperatures during specimen preparation. Note the granular feature throughout the structure; in some areas there is a faint cross-hatched or tweed-like appearance (C).

Fig. 9: Electron micrograph of martensite in an Fe-18Ni-0.40C alloy aged at 100°C for one hour. Substantial areas exhibiting the cross-hatched or tweed-like strain contrast effect (C) can be seen. Note also the fine twins (T) in plate martensite.

Fig. 10: Electron micrograph of martensite in an Fe-18Ni-0.40C alloy tempered at 150°C for one hour. Arrays of very fine carbide particles can be seen in most areas, while in others particles too small to resolve individually apparently give rise to a strain contrast effect (S). Martensite twinning (T) is also shown.

Fig. 11: Electron micrograph of martensite in an Fe-21Ni-0.40C alloy tempered at 200°C for one hour. Well-developed arrays of ε-carbide particles are present. Note areas of coarser granular strain contrast (G) compared to Fig. 8.

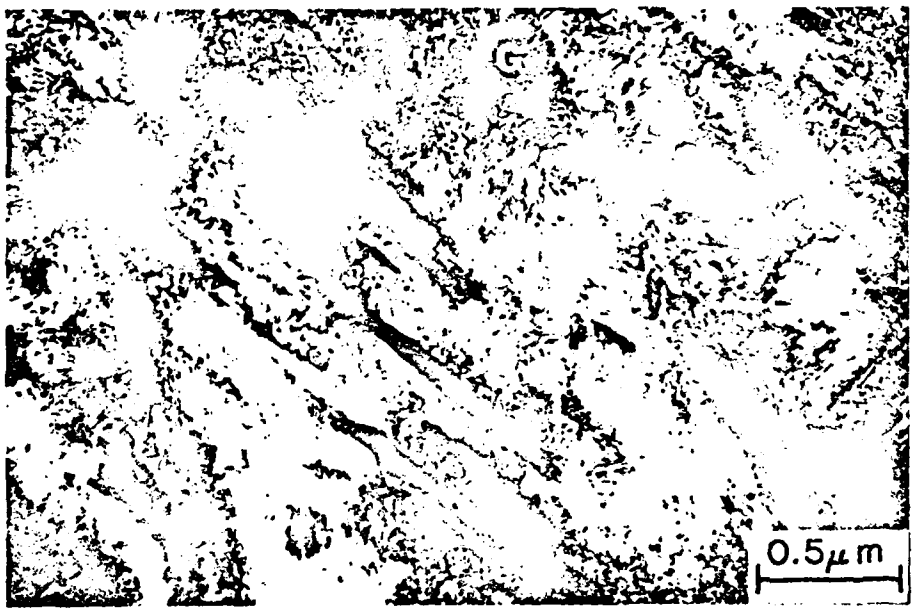

Fig. 12: Electron micrograph of martensite in an Fe-21Ni-0.40C alloy tempered at 300°C for one hour. Large cementite particles are evident, as are areas of coarse granular strain contrast (G) attributable to dislocation tangles.

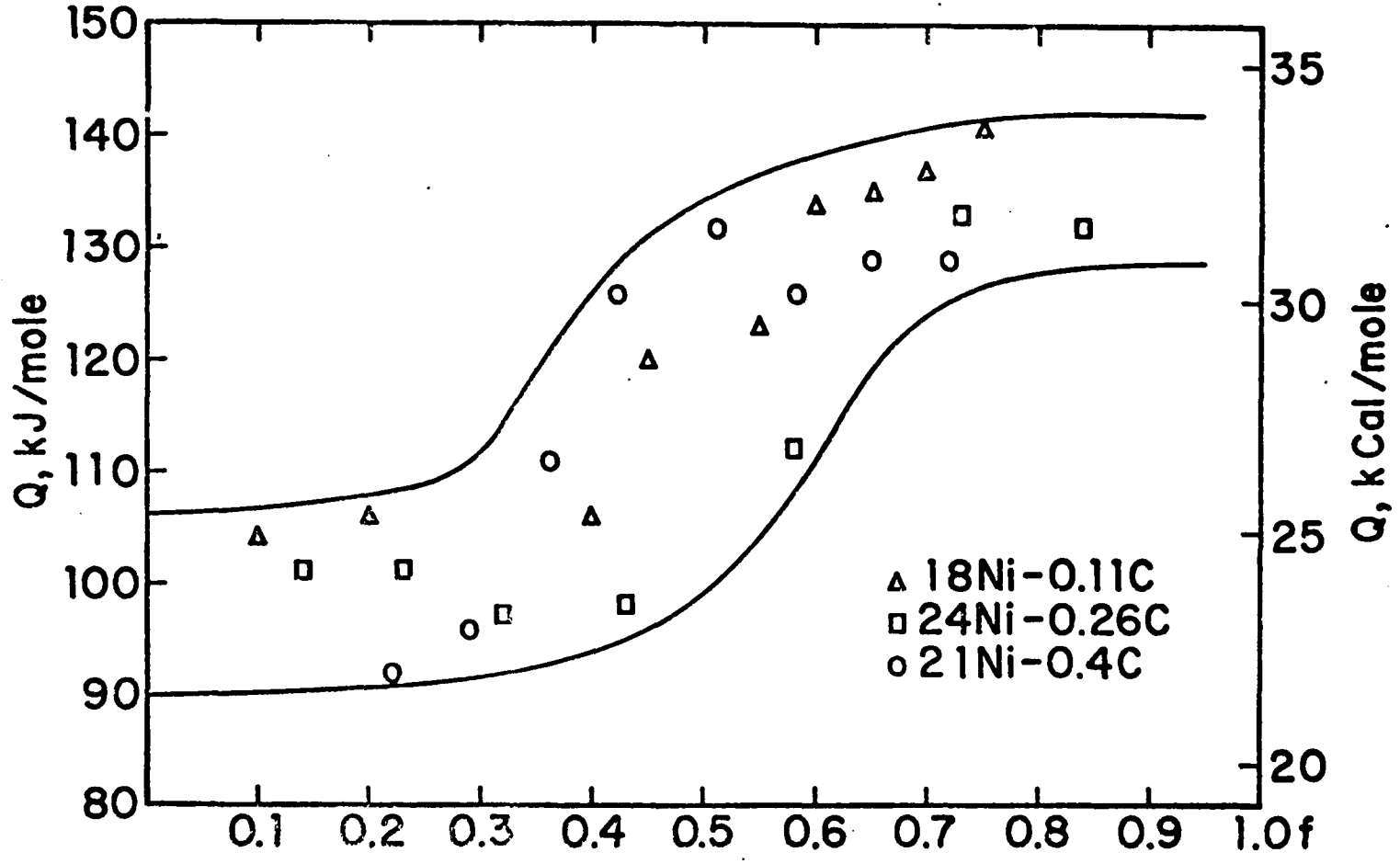

Fig. 13: Activation energy vs. fraction of the total resistivity decrease in Regimes II and III for lath martensite (Fe-18Ni-0.11C) and plate martensite Fe-24Ni-0.26C and Fe-21Ni-0.40C.

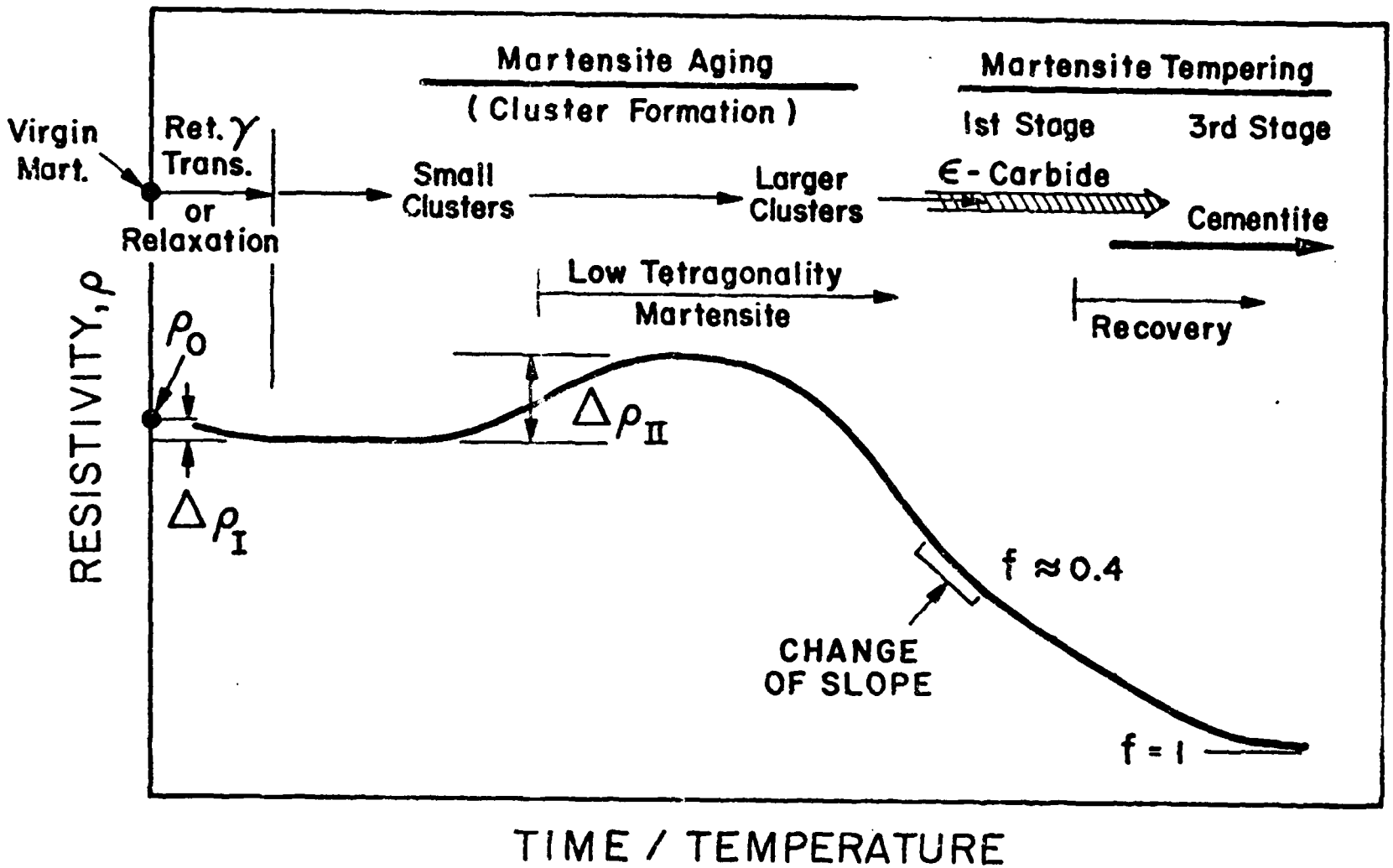

Fig. 14: Schematic summary of structural changes during the aging and tempering of virgin martensites, correlated with the accompanying resistivity changes.


FILMED
8